Journal of Magnetic Resonance 221 (2012) 24–31

Contents lists available at SciVerse ScienceDirect

Journal of Magnetic Resonance

journal homepage: www.elsevier.com/locate/jmr

A spin echo sequence with a single-sided bipolar diffusion gradient pulse to obtain snapshot diffusion weighted images in moving media

R.Z. Freidlin [a,*], J.W. Kakareka [a], T.J. Pohida [a], M.E. Komlosh [b], P.J. Basser [b]

[a] Division of Computational Bioscience, Center for Information Technology, National Institutes of Health, Bethesda, MD, United States
[b] Section on Tissue Biophysics and Biomimetics, Eunice Kennedy Shriver National Institute of Child Health and Human Development, National Institutes of Health, Bethesda, MD, United States

ARTICLE INFO

Article history:
Received 20 December 2011
Revised 30 March 2012
Available online 28 April 2012

Keywords:
Motion artifacts
DWI
DTI
Heart
Spinal cord
Diffusion
MRI

ABSTRACT

In vivo MRI data can be corrupted by motion. Motion artifacts are particularly troublesome in Diffusion Weighted MRI (DWI), since the MR signal attenuation due to Brownian motion can be much less than the signal loss due to dephasing from other types of complex tissue motion, which can significantly degrade the estimation of self-diffusion coefficients, diffusion tensors, etc. This paper describes a snapshot DWI sequence, which utilizes a novel single-sided bipolar diffusion sensitizing gradient pulse within a spin echo sequence. The proposed method shortens the diffusion time by applying a single refocused bipolar diffusion gradient on one side of a refocusing RF pulse, instead of a set of diffusion sensitizing gradients, separated by a refocusing RF pulse, while reducing the impact of magnetic field inhomogeneity by using a spin echo sequence. A novel MRI phantom that can exhibit a range of complex motions was designed to demonstrate the robustness of the proposed DWI sequence.

Published by Elsevier Inc.

1. Introduction

Motion artifacts are a serious confound for *in vivo* phase contrast and amplitude MRI studies. In phase contrast MRI motion causes phase offsets and ghosting in phase maps, distorting measured displacement profiles, and velocity maps. In amplitude MRI, intravoxel motion velocity distributions and shearing motion lead to signal loss. For example, in diffusion MRI, velocity shear within a voxel causes signal attenuation that appears like diffusion (pseudo-diffusion) but is not caused by Brownian motion [1]. The brainstem and spinal cord move significantly during the cardiac cycle, and are particularly troublesome to image. Although DTI data has been collected in human and animal hearts [2–8], reproducible DTI in the beating heart still remains an illusive goal. Whole body diffusion MRI is becoming increasingly important with the recognition that one can detect and possibly stage tumors using diffusion MRI [9]. However, significant motion in the abdomen and gut can hamper the interpretation of DWI data in these soft tissues.

Moreover, there are a number of promising High Angular Resolution Diffusion Imaging (HARDI) [10] sequences that can provide additional information about tissue microstructure and microarchitecture, which are also based on acquiring a large number of DWIs. In these methods, the tissue occupying each voxel is presumed to be the same in each DWI. However, this assumption can seldom be satisfied with existing DWI methods. This is one reason why HARDI-based methods have been applied largely to relatively slowly moving organs and tissue, like the brain, and not more generally, particularly to the beating heart. A snapshot DWI sequence would address these and other important needs within the imaging community.

We have also developed an MR phantom capable of controlling the motion of a specimen that can be used to test a DWI sequence's sensitivity to complex motion. Generally, it has been difficult to compare and contrast different motion control strategies in MRI and to reliably produce and reproduce different motion artifacts and assess their relative severity. An important development would be a controllable MRI phantom that can exhibit a range of complex motions to test the susceptibility of MRI sequences to various motion artifacts and evaluate the efficacy of different correction strategies to mitigate them.

2. Background

2.1. Conventional Stejskal–Tanner DWI sequences

The most common method for sensitizing magnitude MRI data to the effects of water diffusion is by incorporating the Stejskal–Tanner pulsed gradient NMR sequence into a spin-echo (PGSE) MRI sequence [11–14]. Specifically, the spin echo is formed by applying a

* Corresponding author.
E-mail address: raisa@helix.nih.gov (R.Z. Freidlin).

1090-7807/$ - see front matter Published by Elsevier Inc.
http://dx.doi.org/10.1016/j.jmr.2012.04.010

90° RF pulse followed by a 180° RF pulse. Diffusion weighting is obtained by applying a pair of identical unipolar gradient pulses around the slice selective 180° RF pulse (Fig. 1a). These unipolar diffusion-sensitizing gradients induce diffusion-related signal attenuation in tissues as described in Eq. (1). Signal attenuation caused by phase dispersion from diffusion or the random motion of incoherently moving spins enables one to estimate the water diffusivity in each voxel, using:

$$S(b) = S(0)e^{-bD}, \tag{1}$$

where $S(b)$ is the observed signal, $S(0)$ is a signal in the absence of the diffusion-sensitizing gradients, D is the apparent diffusion coefficient (ADC), and b is given by:

$$b = \gamma^2 G^2 \delta^2 \left[\Delta - \frac{\delta}{3}\right], \tag{2}$$

where G is the magnitude of the diffusion gradient pulse with duration δ, and diffusion time Δ [15].

Meanwhile, coherently moving spins (bulk motion in which there is a uniform velocity) produce a constant phase shift [16] in the Stejskal–Tanner pulsed field gradient (PFG) SE sequence:

$$S(\sigma)_{\upsilon} = S(\sigma)e^{-i2\pi\sigma}, \tag{3}$$

where σ is a function of the gradient strength, G, the diffusion timing parameters, δ and Δ; velocity, υ, and is calculated according to:

$$\sigma = \gamma G \delta \Delta \upsilon. \tag{4}$$

It can be seen from Eq. (4) that in the presence of motion as the diffusion time, Δ, gets longer, it is less likely for the family of spins tagged by the first diffusion-sensitizing gradient, which corresponds to a particular anatomical location, to be refocused by the second one, since the tissue has moved, thus introducing a constant phase shift.

2.2. Motion correction strategies for obtaining DWIs in moving media

A number of techniques have been proposed to minimize signal attenuation due to bulk motion during DWI acquisition.

A gradient echo MRI sequence, a special case of the Stejskal–Tanner pulse sequence, consists of a single bipolar gradient block played out after the 90° RF pulse, where the interval between diffusion-sensitizing gradients, Δ, is set to δ (Fig. 1b). Since the dura-

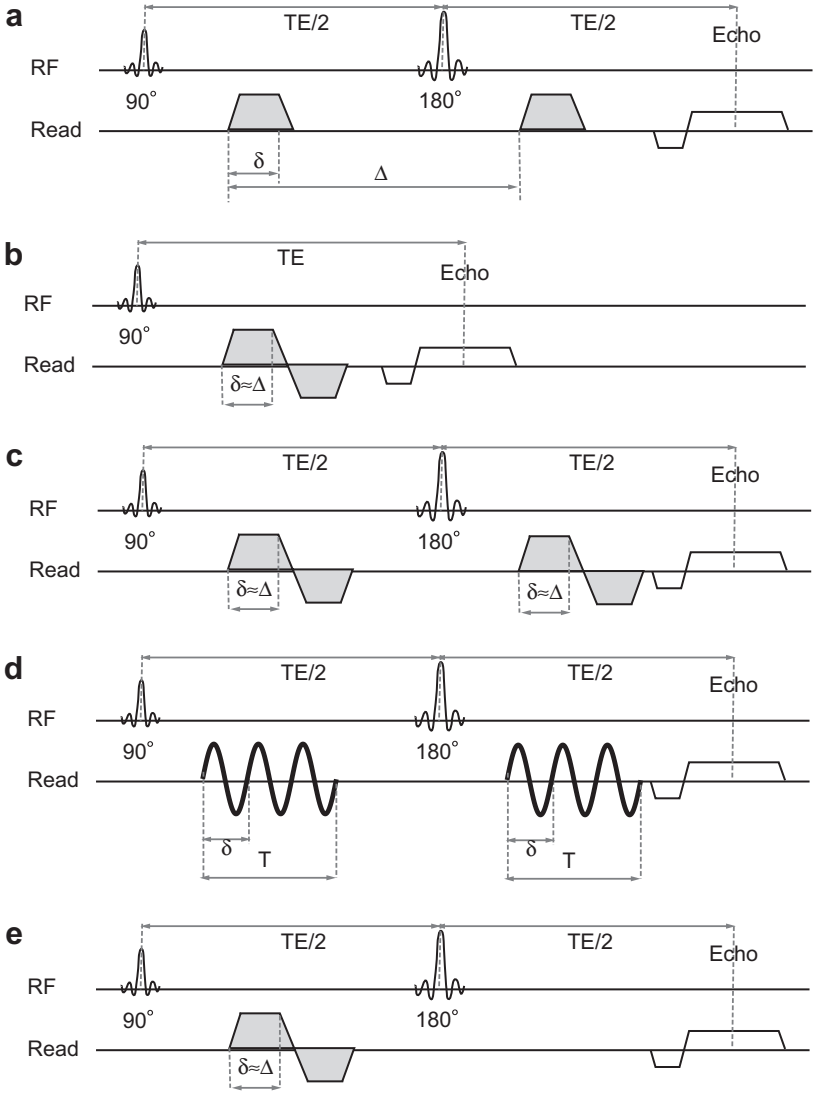

Fig. 1. (a) Stejskal–Tanner, (b) conventional bipolar gradient echo, (c) conventional bipolar spin echo, (d) oscillating gradient spin echo, and (e) single-sided bipolar before refocusing 180° RF pulse DWI sequences.

tion of the diffusion-sensitizing gradients, in general, is shorter than the diffusion time ($\delta < \Delta$), the effect of coherently moving spins is reduced, compared to the conventional PGSE sequence. The b-value for a single bipolar gradient is given in Eq. (5) [17]:

$$b = \frac{2}{3}\gamma^2 G^2 \delta^3, \tag{5}$$

and the velocity sensitive phase variable in Eq. (3) reduces to:

$$\sigma = \gamma G \delta^2 \upsilon. \tag{6}$$

However, despite a shorter echo time and the reduced effect of the diffusion time, this technique is highly sensitive to magnetic field inhomogeneity, and suffers from a significant signal loss due to a shorter T_2^* relaxation time.

In their work, Hong and Dixon [18] demonstrated how replacing the unipolar diffusion-sensitizing gradients in the conventional Stejskal–Tanner with two bipolar diffusion-sensitizing gradient blocks (Fig. 1c) decreases spin dephasing due to magnetic field inhomogeneity, as well as reducing sensitivity to bulk motion. The b-value for the two consecutive bipolar diffusion-sensitizing gradient blocks is:

$$b = \frac{4}{3}\gamma^2 G^2 \delta^3. \tag{7}$$

Although, the bipolar diffusion-sensitizing (BP) sequence appears to be useful for compensating for the coherently moving spins and is cross-term free in regards to the imaging gradients, in real experiments it is impossible to reduce the times between two consecutive bipolar gradients to δ, due to the duration of the 180° RF pulse, as well as the duration of the crushers on both sides of the slice selective refocusing RF pulse. Once again, this sequence suffers from a prolonged time between two consecutive bipolar gradients and the possibility that the medium has moved between the application of the two diffusion gradient pulse blocks.

It is important to note that the effect of the reversed bipolar-sensitizing gradients [18] is similar to the PGSE sequence, since it is not free of cross-term caused by imaging gradients. Hong and Dixon [18] showed that in the presence of such cross-terms the error in the diffusion coefficient calculations is increased.

Another interesting approach to shorten the diffusion time is the oscillating gradient spin echo sequence [19] (OGSE). As shown in Fig. 1d, OGSE is similar to a conventional BP sequence, where the bipolar diffusion-sensitizing gradients are replaced by sinusoidally oscillating gradients with number of cycles, n, with period T (each cycle behaves like a bipolar gradient). The b-value for an oscillating gradient is calculated according to Eq. (8):

$$b = \frac{3}{4}\gamma^2 G^2 \frac{\delta^3}{\pi^2 n^2}, \tag{8}$$

where δ is a duration of the gradient pulse and n is a number of cycles. As the conventional BP sequence, OGSE has the same shortcoming, i.e., a prolonged time between two consecutive oscillating gradients. Thus, it is not suitable in the presence of complex motion.

Cardiac and respiratory triggering techniques [20,21] are relatively successful for suppressing artifacts arising from such quasi-periodic bulk motion as cardiac and cerebrospinal fluid pulsation, and respiratory motion. However, triggering is not as effective for remedying motion artifacts in DWIs of cardiac tissue itself and/or spinal cord, due to uncertainty of the organ's position after each cardiac cycle.

Other motion-remediation approaches are based on navigator echo correction [22,23], where phase correction is performed during post-processing. Once again, such approaches are not efficient for cardiac and spinal imaging due to a number of assumptions about tissue location during acquisition. Thus, the most efficient and logical time to reduce the influence of coherently moving spins is during the acquisition itself.

3. Theory

3.1. Single-sided bipolar gradient spin echo DWI sequences

In this work we propose a novel idea of applying only one bipolar diffusion-sensitizing gradient (Fig. 1e), rather than two on both sides of the slice selective 180° RF pulse in the spin echo DWI sequence. This approach minimizes the effect of the magnetic field inhomogeneity one observes in the gradient echo DWI sequence, and reduces the influence of the coherently moving spins by shortening the time between consecutive diffusion-sensitizing gradients. Although commonly used bipolar DW sequences have a diffusion time, Δ, set to the duration of the diffusion-sensitizing pulse, δ, the time between consecutive bipolar diffusion-sensitizing gradients in the moving media causes motion artifacts. Since the diffusion-sensitizing gradients are the leading source of phase dispersion, it is extremely important to minimize the impact of dephasing due to bulk motion not just during, but especially in between these gradients. These new single-sided bipolar spin echo (SS-BPSE) DWI sequences utilize minimum diffusion gradient separation, while reducing signal attenuation due to T_2^* relaxation.

As in the case of the gradient echo sequence, b-values are calculated according to Eq. (5). For other than the rectangular shaped diffusion-sensitizing gradients, the calculations of b-values or b-matrices [24] have to be modified according to the shape of the pulses [25].

Although applying a single bipolar gradient block significantly reduces the diffusion weighting as compared to the conventional "two-sided" bipolar or unipolar diffusion-sensitizing sequences, it is still possible using current clinical gradient hardware to generate b-values adequate for cardiac tissue ($b \approx 400$ s/mm^2) [7] and spinal cord DWI ($b \approx 500$ s/mm^2) [26].

Another major advantage of the bipolar diffusion-sensitizing waveform is elimination of the residual eddy currents [17]. Since the lobes of this gradient are of opposite polarity, eddy currents are largely refocussed.

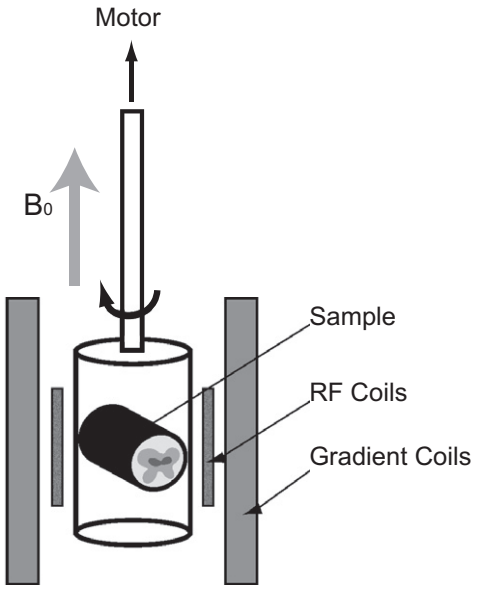

Fig. 2. Schematic drawing of the experimental setup.

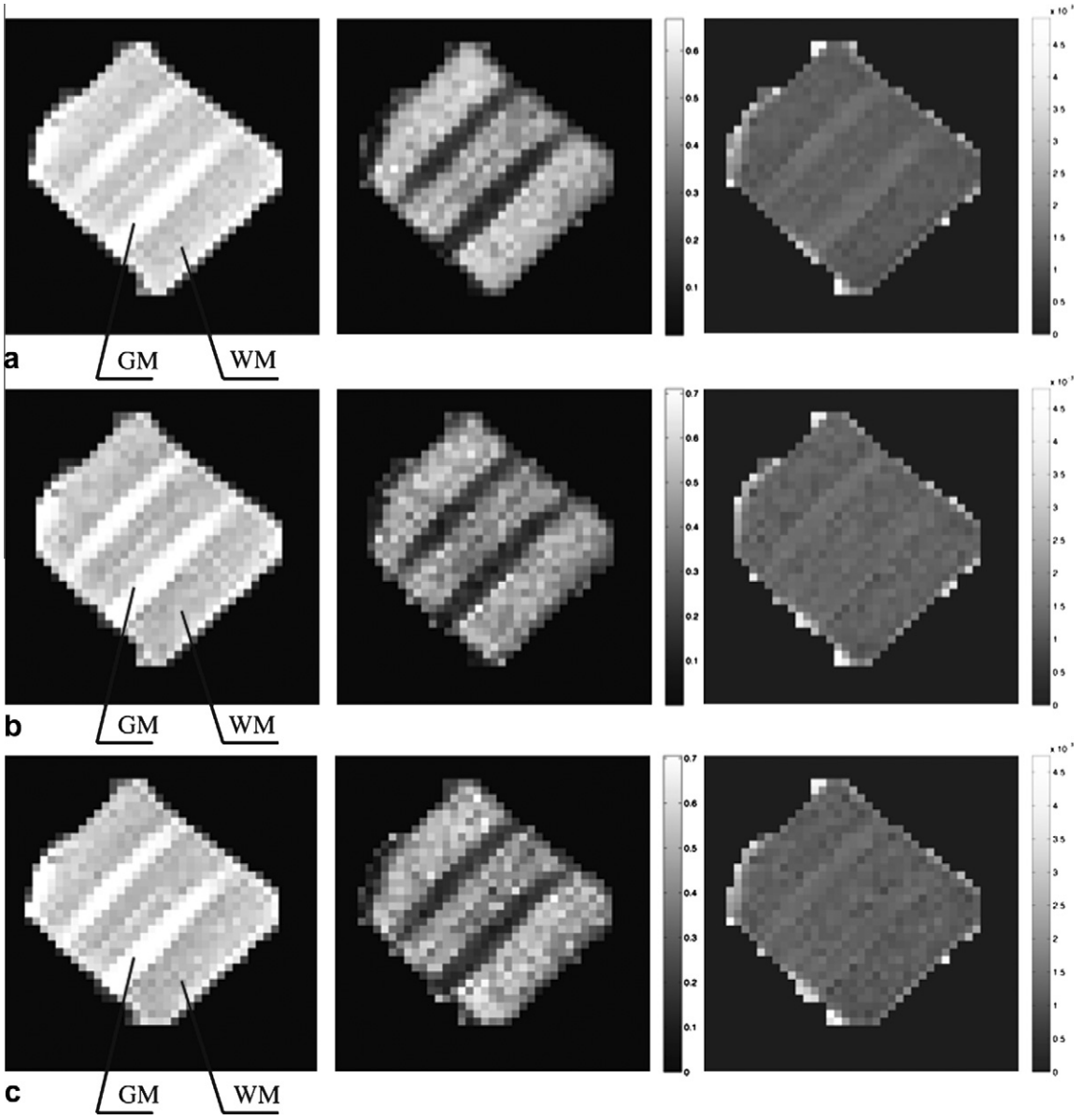

Fig. 3. A (0) (GM – gray matter, WM – white matter), *FA*, and $Tr \times 10^{-3}$ mm^2/s maps of the stationary excised pig spinal cord sample obtained with (a) PGSE, (b) conventional BP, and (c) SS-BPSE sequences.

4. Materials and methods

4.1. Rotating MRI phantom

A Bruker Rheo-NMR [27] unit consists of an MR compatible rotating shaft driven by an integrated stepper motor/controller unit that imparts a continuous angular motion to a "cone and plate" or Couette flow cell within a Micro2.5 microscopy probe (25 mm solenoid coil). We cannibalized this apparatus, replacing the motor and controller unit so that the shaft and fixture can exhibit arbitrarily rotational complex, jerky motions. A custom module allows the user to prescribe arbitrary shaft rotation waveforms based on a trigger input, including motionless periods. A combination of rotational acceleration and motionless periods (pause in rotation) during each cycle simulates jerky motions in the heart. Another important feature of this apparatus is that this complex motion can be triggered to the acquisition of the MRI sequence. We also developed specialized fixtures to hold different tissues to be scanned, see Fig. 2. The specimen holder allows for a tissue plug to be inserted. Susceptibility effects can be minimized by potting the specimen in perfluoropolyether oil ("Fomblin"). The fixture itself is constructed from ULTEM, a susceptibility matched plastic.

4.2. Excised pig spinal cord DTI experiments

To test whether the proposed SS-BPSE PFG MRI sequence reduces motion artifacts in moving media as compared to the PGSE and BP sequences, we obtained different DWI data from the same excised pig spinal cord fixed with 4% paraformaldehyde solution. Prior to DWI data collection, the spinal cord was washed in phosphate-buffered saline (PBS) doped with Gd-DTPA. Gadolinium was used to decrease the T_1 relaxation time of the spinal cord tissue. The sample was imaged in the modified "cone and place" cell from the RheoNMR cell kit filled with Fomblin, within a vertical-bore 7T Bruker (Germany) scanner fitted with Micro2.5 microscopy probe (25 mm solenoid coil) with 1450 mT/m 3-axis gradients (Fig. 2). The common parameters for PGSE, conventional BP, and SS-BPSE

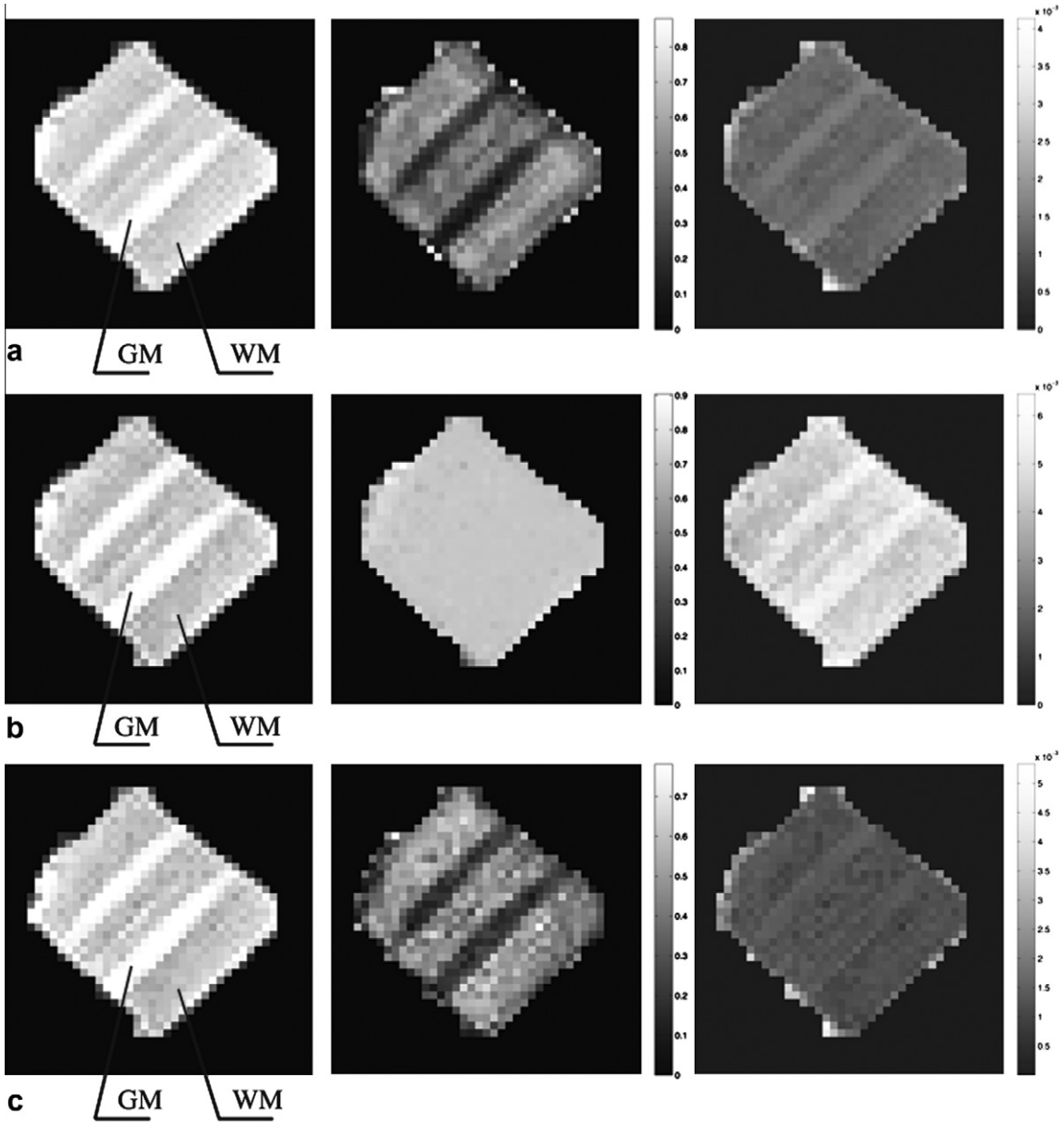

Fig. 4. A (0) (GM - gray matter, WM - white matter), *FA*, and $Tr \times 10^{-3}$ mm^2/s maps of the rotating excised pig spinal cord sample obtained with (a) PGSE, (b) conventional BP, and (c) SS-BPSE sequences (GM – gray matter, WM – white matter).

sequences include repetition time (TR) = 800 ms, bandwidth = 100 kHz, field-of-view (FOV) = 20 × 20 mm, matrix = 64 × 64 with a 1-mm thick axial slice. PGSE echo time (TE) was set to 26 ms, while both BP and SS-BPSE had TE set to 37 ms. One DWI per slice was acquired with $b \approx 0$ s/mm^2, followed by 21 DWIs with $b = 1200$ s/mm^2. DWIs were acquired: (1) without rotation and (2) with rotation at 1 Hz and 15 ms motor pause. The diffusion gradient duration, δ, was 8 ms and the gradient separation, Δ, was 10.2 ms for PGSE and $\delta = 8$ ms and $\Delta = 8$ ms for conventional BP and SS-BPSE, respectively. The same diffusion-sensitizing gradient duration was chosen in order to show the impact of separation (duration of 180° RF pulse and spoilers around it) between unipolar and bipolar gradients in PGSE and BP sequences, respectively. Although reducing a diffusion gradient duration for PGSE and BP sequence decreases the diffusion time, this separation remains constant.

At each voxel location in the raw image, the apparent diffusion tensor, $\overline{\mathbf{D}}$, was estimated from the acquired DWIs and tensor-derived parameters, such as the eigenvectors or principal directions, ϵ_1,ϵ_2, and ϵ_3, and the corresponding eigenvalues or principal diffusivities, λ_1, λ_2, and λ_3, were estimated [28]. These were passed to parsimonious model selection [29] and multivariate hypothesis testing clustering [30] algorithms.

5. Results

5.1. Comparison of SS-BPSE with PGSE and conventional BP

As can be seen in Fig. 3, the results were highly consistent for all three evaluated sequences for the stationary sample of the excised pig spinal cord, although the *SNR* was better for PGSE sequences due to a shorter echo time. For this particular sample, the average fractional anisotropy, *FA*, in white matter was around 0.48, while trace of the diffusion tensor, *Tr*, was approximately 1.3×10^{-3} mm^2/s. However, for the rotating sample, results obtained with the BP sequence (Fig. 4b) were quite different from the results obtained with PGSE and SS-BPSE (Fig. 4a and c, respectively), i.e.,

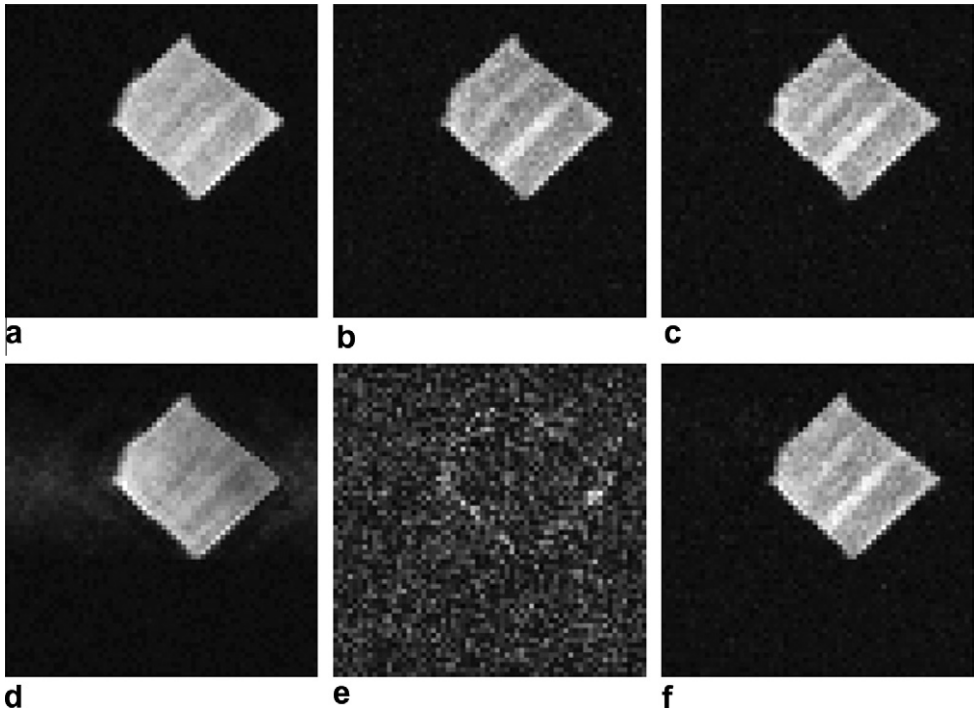

Fig. 5. Diffusion-weighted images along one direction of the stationary excised pig spinal cord sample obtained with (a) PGSE, (b) conventional BP, and (c) SS-BPSE sequences; and of the rotating excised pig spinal cord sample obtained with (d) PGSE, (e) conventional BP, and (f) SS-BPSE sequences.

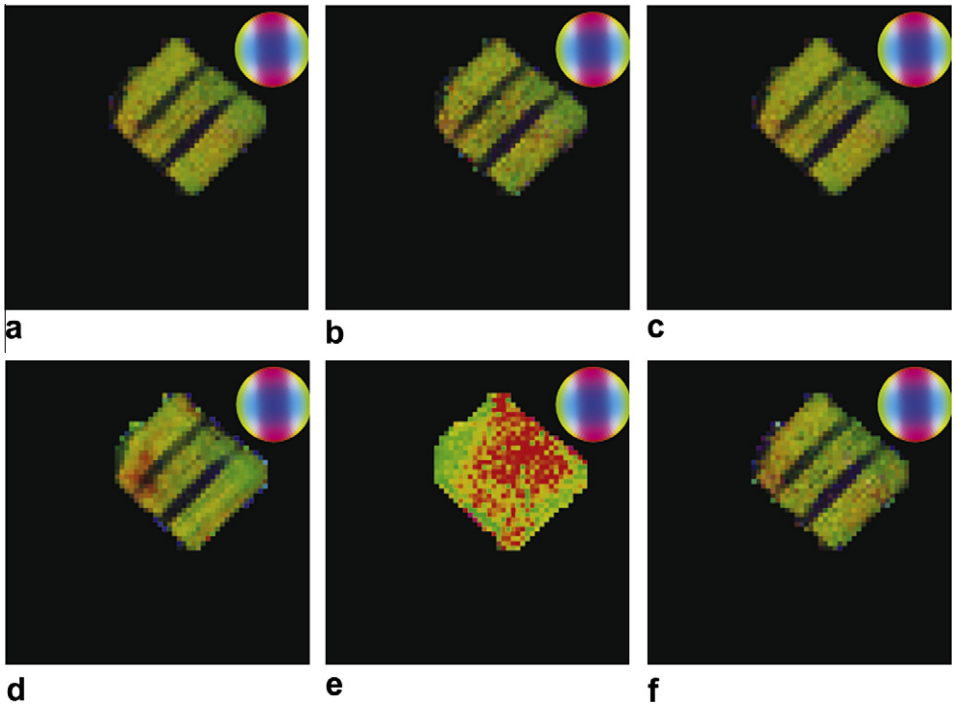

Fig. 6. Direction encoded color maps of the stationary excised pig spinal cord sample obtained with (a) PGSE, (b) conventional BP, and (c) SS-BPSE sequences; and of the rotating excised pig spinal cord sample obtained with (d) PGSE, (e) conventional BP, and (f) SS-BPSE sequences. Color hue represent directions as: green is left–right, red is up–down, and blue is through the plane.

$FA \approx 0.71$ and $Tr \approx 4.5 \times 10^{-3}$ mm^2/s for the BP sequence, while for both PGSE and SS-BPSE $FA \approx 0.49$ and $Tr \approx 1.3 \times 10^{-3}$ mm^2/s.

Although results for the rotating sample obtained with PGSE and SS-BPSE sequences appear to be similar, after further examination of the individual DWIs (the examples of the DWIs for one direction are given in Fig. 5a–c for stationary, and d, e, and f for rotating samples, respectively), it becomes clear that motion artifacts are more pronounced in PGSE images (Fig. 5d) compared to SS-BPSE images (Fig. 5f).

Furthermore, evaluation of the Direction Encoded Color maps [31] shows that the result obtained with PGSE (Fig. 6a and d) and BP sequences (Fig. 6b and e) are not consistent between

stationary and rotating experiments. Alternatively, the SS-BPSE sequence produces compatible results for both stationary and rotating experiments (Fig. 6c and f, respectively).

Fig. 7a and b show clusters of homogeneous tissue obtained from the measured DTI field maps obtained with PGSE and SS-BPSE sequences for the stationary sample. As can be seen, both sequences produced consistent results in white matter. However, in the rotating experiment, due to averaging caused by motion, the clustering algorithm fails to distinguish white and gray matter in the spinal cord (Fig. 7c). The SS-BPSE sequence successfully separates white and gray matter (Fig. 7d); however, there are slight variations in the degree of homogeneity in white matter (the different colors within the white matter identify three separate clusters).

6. Discussion

In this work we show that in the presence of complex motion, the SS-BPSE sequence outperforms both PGSE and the conventional BP sequences. Especially poor performance of the conventional BP sequence in the presence of jerky motion can be explained by the fact that this sequence is flow compensating only. In other words, if tissue experiences different types of motion (stopping and starting) during the bipolar gradients applied before and after the 180° RF pulse, dephasing can lead to a significant signal loss along some diffusion-sensitizing directions (Fig. 5e). As has been mentioned before, the same *b*-value for all three sequences was achieved by varying the strength of the diffusion gradient, rather than its duration. In the presence of jerky motion, varying the duration of the diffusion gradients instead of their amplitudes did not achieve a significant improvement for the PGSE and the conventional BP sequences compared to SS-BPSE. This can be attributed to an insufficient duration reduction, since for the PGSE and the conventional BP sequences the durations could be reduced only by ~14% and ~20% compared to SS-BPSE, respectively. Such reduction is not sufficient for minimizing jerky motion artifacts when the two diffusion-sensitizing gradients, either unipolar or bipolar, are separated by the refocusing 180° RF pulse with spoilers around it. The advantages of SS-BPSE are especially pronounced as resolution is reduced since velocity shear within a voxel is more pronounced as the voxel size increases [1]. It is important to note that PGSE has better *SNR* due to shorter TE and requires less diffusion gradient strength to achieve diffusion weighting comparable to SS-BPSE and conventional BP.

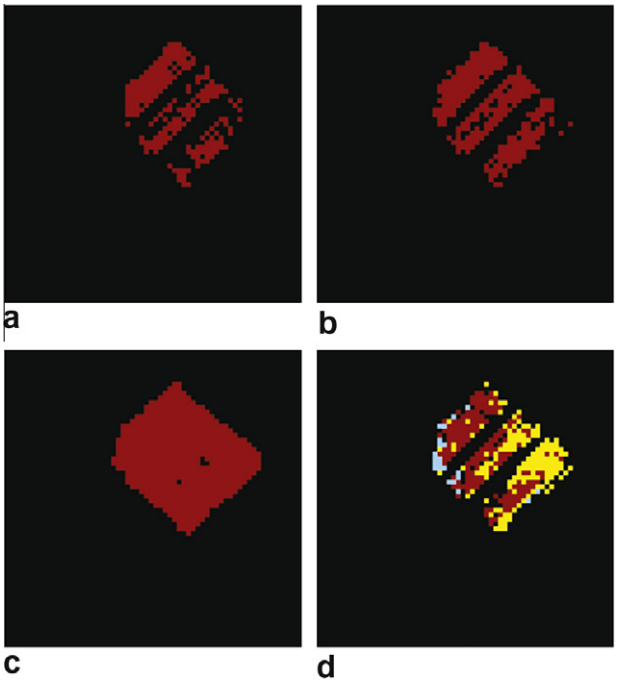

Fig. 7. Clusters, which identified homogeneity of the measured DTI field maps of the stationary excised pig spinal cord sample obtained with (a) PGSE and (b) SS-BPSE sequences; and the rotating excised pig spinal cord sample obtained with (c) PGSE and (d) SS-BPSE sequences. The discrete colors within white matter correspond to separate clusters with a different degree of homogeneity.

This new DWI sequence is potentially useful in many application areas. Clearly, there is a need to perform diffusion MRI studies in the beating heart; this goal has been illusive since the invention of diffusion MRI. DTI in the beating heart will enable the assessment of muscle fiber structure and architectural organization in the heart wall as well as the acquisition of mean ADC estimates in cardiac muscle tissue. The mean ADC could be calculated from the estimated diffusion tensor itself, from several ADCs obtained in an isotropically organized DWI acquisition, or by using an isotropically weighted DWI sequence. This information should be useful in identifying abnormal or ischemic areas of the heart.

Increasingly, there are reports of intravoxel incoherent motion (IVIM) [32] in living tissues, particularly in highly perfused tissues like kidney [33] and liver [34]. IVIM effects have been reported in *b*-value ranges of 0 to approximately 100 s/mm^2. Some of the observed IVIM effect may be due to complex organ and tissue motion and deformations in addition to the presumed capillary and extracellular fluid flow assumed in the IVIM theory. This new DWI acquisition framework may reduce this artifactual contribution to the IVIM effect, and allow a closer examination of the IVIM perfusion effects if they exist.

Another area of intense interest in the neuroimaging community is the assessment of spinal cord and the brainstem. It is extremely challenging to obtain DWIs in these structures owing to the significant side-to-side "whip" of the spinal cord and the plunging motion of the brainstem. We expect that the ability to measure of diffusion rapidly will improve the assessment of these important structures.

There are clearly several potential embodiments of this DWI sequence that have advantages for particular applications. The diffusion spectroscopic SE sequence could be used as an NMR prefilter prior to the application of an MRI block. The diffusion gradient pulse could be used within a conventional SE sequence with slice select and phase encode gradients applied. For isotropically weighted DWIs the same principle holds. The isotropically weighted spectroscopic SE sequence can be applied as a filter to an MRI block or incorporated within an MRI block.

In general, there is a large and growing family of DWI methods that do not use the ADC or DTI models to obtain useful information about tissue microstructure and architecture. High Angular Resolution Diffusion Imaging (HARDI) [10] acquisitions arise in many higher order diffusion MRI applications. Examples include Q-ball MRI [35], PAS MRI [36], DOT [37], Generalized DTI [38,39], etc. Other methods of analyzing DWI data that are not model specific, such as *k*- and *q*-space MRIs [40], Diffusion Spectrum MRI (DSI) [41], and SHORE 3D [42], which attempt to measure the average propagator directly from the DWI data, also can employ these new DWIs to improve data fidelity. Such applications should become more feasible particularly as gradient hardware improves, i.e., gradient strength and slew-rate increases.

A possible extension of this method for obtaining DWIs is to use the bipolar gradient acquisition scheme above in multiple wavevector or multiple pulsed gradient field (mPFG) NMR and MRI measurements []. Research indicates the measurements may be very useful in identifying features of microstructure within tissues and other media without requiring strong diffusion gradients

[43]. In these mPFG applications at least two Stejskal and Tanner single PFG blocks are concatenated to produce a multiple PFG MR sequence. The single sided bipolar PFG sequence can replace the two Stejskal–Tanner gradient pulses to obtain this novel type of diffusion weighting.

7. Conclusion

This new DW sequence is designed to fill a critical need for measuring diffusion parameters over short time periods in presence of tissue motion, both accurately and robustly. Our intent is to continue to develop and apply this snapshot DWI sequence in a variety of *in vivo* applications where motion makes conventional DWI acquisitions problematic.

Acknowledgments

R.Z.F thanks Kenneth Kempner and Dr. Benes Trus for their support and encouragement. The authors thank Drs. Alexandru Avram, Martin Lizak, and Joelle Sarlls for helpful discussions and Liz Salak for editing this paper. We would also like to thank the those who were involved in providing this research with the pig spinal cord tissue: Mr. R.R. Clevenger, Mr. T.J. Hunt, Ms. G.J. Zywicke, Mr. A.D. Zetts, Mrs. K. Keeran, Mr. S.M. Kozlov, and Mr. K.R. Jeffries, from LAMS, NHLBI. This research was sponsored by the Intramural Research Program of the Eunice Kennedy Shriver National Institute of Child Health and Human Development and the Center for Information Technology, National Institutes of Health, Bethesda, Maryland.

References

[1] U. Nevo, E. Ozarslan, M.E. Komlosh, C.G. Koay, J.E. Sarlls, P.J. Basser, A system and mathematical framework to model shear flow effects in biomedical DW-imaging and spectroscopy, NMR Biomed. 23 (7) (2010) 734–744, http://dx.doi.org/10.1002/nbm.1591.
[2] T.G. Reese, R.M. Weisskoff, R.N. Smith, B.R. Rosen, R.E. Dinsmore, V.J. Wedeen, Imaging myocardial fiber architecture in vivo with magnetic resonance, Magnet. Reson. Med. 34 (6) (1995) 786–791.
[3] E.W. Hsu, A.L. Muzikant, S.A. Matulevicius, R.C. Penland, C.S. Henriquez, Magnetic resonance myocardial fiber-orientation mapping with direct histological correlation, Am J Physiol 274 (5 Pt 2) (1998) H1627–H1634.
[4] W.Y. Tseng, T.G. Reese, R.M. Weisskoff, V.J. Wedeen, Cardiac diffusion tensor MRI in vivo without strain correction, Magnet. Reson. Med. 42 (2) (1999) 393–403.
[5] J. Dou, T.G. Reese, W.-Y.I. Tseng, V.J. Wedeen, Cardiac diffusion MRI without motion effects, Magnet. Reson. Med. 48 (1) (2002) 105–114, http://dx.doi.org/10.1002/mrm.10188.
[6] P. Helm, M.F. Beg, M.I. Miller, R.L. Winslow, Measuring and mapping cardiac fiber and laminar architecture using diffusion tensor MR imaging, Ann. NY Acad. Sci. 1047 (2005) 296–307, http://dx.doi.org/10.1196/annals.1341.026.
[7] U. Gamper, P. Boesiger, S. Kozerke, Diffusion imaging of the in vivo heart using spin echoes–considerations on bulk motion sensitivity, Magnet. Reson. Med. 57 (2) (2007) 331–337, http://dx.doi.org/10.1002/mrm.21127.
[8] N. Toussaint, M. Sermesant, C.T. Stoeck, S. Kozerke, P.G. Batchelor, In vivo human 3D cardiac fiber architecture: reconstruction using curvilinear interpolation of diffusion tensor images, Med. Image Comput Comput Assist Intervent 13 (Pt 1) (2010) 418–425.
[9] A.R. Padhani, G. Liu, D.M. Koh, T.L. Chenevert, H.C. Thoeny, T. Takahara, A. Dzik-Jurasz, B.D. Ross, M.V. Cauteren, D. Collins, D.A. Hammoud, G.J.S. Rustin, B. Taouli, P.L. Choyke, Diffusion-weighted magnetic resonance imaging as a cancer biomarker: consensus and recommendations, Neoplasia 11 (2) (2009) 102–125.
[10] D.S. Tuch, R.M. Weisskoff, J.W. Belliveau, V.J. Wedeen, High angular resolution diffusion imaging of the human brain, in: Proceedings of the 7th Annual Meeting of ISMRM, Philadelphia, 1999, p. 321.
[11] E.O. Stejskal, J.E. Tanner, Spin diffusion measurements: spin echoes in the presence of a time-dependent field gradient, J. Chem. Phys. 42 (1) (1966) 288–292.
[12] D.G. Taylor, M.C. Bushell, The spatial mapping of translational diffusion coefficients by the NMR imaging technique, Phys. Med. Biol. 30 (4) (1985) 345–349.
[13] K. Merboldt, H. W, J. Frahm, Self-diffusion NMR imaging using stimulated echoes, J. Magnet. Reson. 64 (3) (1985) 479–486.
[14] D.L. Bihan, E. Breton, D. Lallemand, P. Grenier, E. Cabanis, M. Laval-Jeantet, MR imaging of intravoxel incoherent motions: application to diffusion and perfusion in neurologic disorders, Radiology 161 (2) (1986) 401–407.
[15] G.E. Wesbey, M.E. Moseley, R.L. Ehman, Translational molecular self-diffusion in magnetic resonance imaging. i. effects on observed spin-spin relaxation, Invest. Radiol. 19 (6) (1984) 484–490.
[16] E.L. Hahn, Detection of sea-water motion by nuclear precession, J. Geophys. Res. 65 (2) (1960) 776–777.
[17] A.L. Alexander, J.S. Tsuruda, D.L. Parker, Elimination of eddy current artifacts in diffusion-weighted echo-planar images: the use of bipolar gradients., Magnet. Reson. Med. 38 (6) (1997) 1016–1021.
[18] X. Hong, W.T. Dixon, Measuring diffusion in inhomogeneous systems in imaging mode using antisymmetric sensitizing gradients, J. Magnet. Reson. 99 (3) (1992) 561–570, http://dx.doi.org/10.1016/0022-2364(92)90210-X.
[19] B. Gross, R. Kosfeld, Application of Spin-Echo method in measurement of auto-diffusion, Messtechnik 77 (7–8) (1969) 171–177.
[20] D. Chien, R.B. Buxton, K.K. Kwong, T.J. Brady, B.R. Rosen, MR diffusion imaging of the human brain, J. Comput. Assist. Tomogr. 14 (4) (1990) 514–520.
[21] C. Thomsen, O. Henriksen, P. Ring, In vivo measurements of relaxation process in the human liver by MRI. the role of respiratory gating/triggering, Magnet. Reson. Imag. 6 (4) (1988) 431–436.
[22] R.J. Ordidge, J.A. Helpern, Z.X. Qing, R.A. Knight, V. Nagesh, Correction of motional artifacts in diffusion-weighted MR images using navigator echoes, Magnet. Reson. Imag. 12 (3) (1994) 455–460.
[23] A.W. Anderson, J.C. Gore, Analysis and correction of motion artifacts in diffusion weighted imaging, Magnet. Reson. Med. 32 (3) (1994) 379–387.
[24] P.J. Basser, J. Mattiello, D. LeBihan, MR diffusion tensor spectroscopy and imaging, Biophys. J. 66 (1) (1994) 259–267.
[25] J. Mattiello, P.J. Basser, D. LeBihan, Analytical expressions for the b-matrix in NMR diffusion imaging and spectroscopy, J. magnet reson. Series A 108 (2) (1994) 131–141.
[26] J. Renoux, D. Facon, P. Fillard, I. Huynh, P. Lasjaunias, D. Ducreux, MR diffusion tensor imaging and fiber tracking in inflammatory diseases of the spinal cord, AJNR Am. J. Neuroradiol. 27 (9) (2006) 1947–1951.
[27] P. Callaghan, Rheo-NMR: nuclear magnetic resonance and the rheology of complex fluids, Rep Prog Phys 62 (4) (1999) 599–670.
[28] P.J. Basser, J. Mattiello, D. LeBihan, Estimation of the effective self-diffusion tensor from the NMR spin echo, J. Magnet. Reson. B 103 (3) (1994) 247–254.
[29] R.Z. Freidlin, E. Ozarslan, M.E. Komlosh, L.-C. Chang, C.G. Koay, D.K. Jones, P.J. Basser, Parsimonious model selection for tissue segmentation and classification applications: a study using simulated and experimental DTI data, IEEE Trans. Med. Imaging 26 (11) (2007) 1576–1584, http://dx.doi.org/10.1109/TMI.2007.907294.
[30] R.Z. Freidlin, E. Ozarslan, Y. Assaf, M.E. Komlosh, P.J. Basser, A multivariate hypothesis testing framework for tissue clustering and classification of DTI data, NMR Biomed 22 (7) (2009) 716–729, http://dx.doi.org/10.1002/nbm.1383.
[31] S. Pajevic, C. Pierpaoli, Color schemes to represent the orientation of anisotropic tissues from diffusion tensor data: application to white matter fiber tract mapping in the human brain, Magnet. Reson. Med. 42 (3) (1999) 526–540.
[32] D.L. Bihan, E. Breton, D. Lallemand, M.L. Aubin, J. Vignaud, M. Laval-Jeantet, Separation of diffusion and perfusion in intravoxel incoherent motion MR imaging, Radiology 168 (2) (1988) 497–505.
[33] M.F. Muller, P.V. Prasad, R.R. Edelman, Can the IVIM model be used for renal perfusion imaging? Eur J. Radiol. 26 (3) (1998) 297–303, http://dx.doi.org/10.1016/S0720-048X(97)01161-3.
[34] A. Luciani, A. Vignaud, M. Cavet, J.T.V. Nhieu, A. Mallat, L. Ruel, A. Laurent, J.-F. Deux, P. Brugieres, A. Rahmouni, Liver cirrhosis: intravoxel incoherent motion MR imaging–pilot study, Radiology 249 (3) (2008) 891–899, http://dx.doi.org/10.1148/radiol.2493080080.
[35] D.S. Tuch, Q-ball imaging, Magnet. Reson. Med. 52 (6) (2004) 1358–1372, http://dx.doi.org/10.1002/mrm.20279.
[36] K.M. Jansons, D.C. Alexander, Persistent angular structure: new insights from diffusion mri data. dummy version., Inf. Process Med. Imaging 18 (2003) 672–683.
[37] E. Özarslan, T.M. Shepherd, B.C. Vemuri, S.J. Blackband, T.H. Mareci, Resolution of complex tissue microarchitecture using the diffusion orientation transform (DOT), NeuroImage 31 (2006) 1086–1103.
[38] E. Özarslan, T.H. Mareci, Generalized diffusion tensor imaging and analytical relationships between diffusion tensor imaging and high angular resolution diffusion imaging, Magnet. Reson. Med. 50 (5) (2003) 955965, http://dx.doi.org/10.1002/mrm.10596.
[39] C. Liu, R. Bammer, B. Acar, M.E. Moseley, Characterizing non-gaussian diffusion by using generalized diffusion tensors, Magnet. Reson. Med. 51 (5) (2004) 924–937, http://dx.doi.org/10.1002/mrm.20071.
[40] P.T. Callaghan, C.D. Eccles, Y. Xia, NMR microscopy of dynamic displacements - k-space and q-space imaging, J. Phys. E-Sci. Instrum. 21 (8) (1988) 820–822.
[41] V.J. Wedeen, P. Hagmann, W.Y.I. Tseng, T.G. Reese, R.M. Weisskoff, Mapping complex tissue architecture with diffusion spectrum magnetic resonance imaging, Magnet. Reson. Med. 54 (6) (2005) 1377–1386.
[42] E. Özarslan, C.G. Koay, T.M. Shepherd, S.J. Blackband, P.J. Basser, Simple harmonic oscillator based reconstruction and estimation for three-dimensional q-space mri, in: Proc. Int. Soc. Magnet. Reson. Med., 2009, p. 1396.
[43] M.E. Komlosh, F. Horkay, R.Z. Freidlin, U. Nevo, Y. Assaf, P.J. Basser, Detection of microscopic anisotropy in gray matter and in a novel tissue phantom using double pulsed gradient spin echo mr, J. Magnet. Reson. 189 (1) (2007) 38–45, http://dx.doi.org/10.1016/j.jmr.2007.07.003.